B Physics Anomalies from Dark Matter

Tomás Costa Lopes
tomasclopes@tecnico.ulisboa.pt

Instituto Superior Técnico, Lisboa, Portugal

October 2022

In this work we study an extension of the Standard Model (SM) by comparing two models which explain the origin of the experimental hints of lepton flavor universality violation in $b \to sl^+l^-$ decays, the long-standing muon $(g-2)$ anomaly and the dark matter (DM) problem. The b decays and the muon $(g-2)$ anomalies are explained by additional one-loop diagrams with DM candidates. Besides the Standard Model fields, the models have a colourless fermion field, a colourless scalar field and a coloured scalar field. In one model, the fermion is an $SU(2)_L$ doublet and the scalars are $SU(2)_L$ singlets, while in the other the fermion is an $SU(2)_L$ singlet and the scalars are $SU(2)_L$ doublets. After studying the dark matter and flavour physics phenomenology of the models, we perform a parameter scan and search for the parameter space of the models which explains all three new physics phenomena simultaneously. We conclude that both models can explain all previously mentioned issues simultaneously while also satisfying other flavour and DM constraints. However, there are crucial differences between how the DM constraints affect the two models, leading to a noticeable difference in the allowed DM mass.

Keywords: new physics model, b quark decay, dark matter, anomalous moment of the muon;

1. Introduction

Although the SM is currently the best theory to describe particle physics, it still leaves some aspects of the universe to be explained (such as neutrino masses, baryon asymmetry in the universe, among other problems), leading us to believe that the theory is in fact incomplete and needs to incorporate new physics (NP) to account for all these observations. One of the main problems at the core of any extension of the Standard Model (SM) is the existence of dark matter (DM). Although it is not at all clear if DM will manifest itself as a particle, this is certainly an avenue of research that is worth exploring. However, there are no restrictions regarding the nature of the DM particle. Not only the allowed mass range is almost unconstrained, but also its quantum numbers are unknown. Therefore, as long as the experimental results are in agreement with the proposed DM candidate in a given model, all possibilities are valid in principle. It would be interesting to have a DM candidate that could also solve discrepancies observed in other and apparently unrelated experiments.

A recent hint of NP is the observed anomaly in the semileptonic decay rate of the B meson, which suggests a violation of lepton flavour universality: the measurement of the ratios of the branching fractions

$$R(K^{(*)}) = \frac{\mathcal{B}(B \to K^{(*)}\mu^+\mu^-)}{\mathcal{B}(B \to K^{(*)}e^+e^-)} \tag{1}$$

was obtained by the LHCb Collaboration [1, 2, 3] with values

$$R(K) = 0.846^{+0.060+0.016}_{-0.054-0.014}, \quad q^2 \in [1,1,6]GeV^2 \tag{2}$$

and

$$R(K^{(*)}) = \begin{cases} 0.660^{+0.110}_{-0.070} \pm 0.024, & q^2 \in [0.045, 1.1]GeV^2 \\ 0.685^{+0.113}_{-0.069} \pm 0.047 & q^2 \in [1.1, 6]GeV^2 \end{cases}, \tag{3}$$

where q^2 is the dilepton mass squared in the process. However, the Standard model predictions [4, 5] are

$$R(K) = 1.0004(8), \quad q^2 \in [1,1,6]GeV^2 \tag{4}$$

and:

$$R(K^{(*)}) = \begin{cases} 0.920 \pm 0.007, & q^2 \in [0.045, 1.1]GeV^2 \\ 0.996 \pm 0.002 & q^2 \in [1.1, 6]GeV^2 \end{cases}. \tag{5}$$

One should note that these experimental results are clean probes of NP: the discrepancies in the values $R(K^{(*)})$ cannot be due to unconsidered QCD effects since the hadronic terms in the expression cancel out [4].

There are also other important hints of new physics like the long-standing low energy flavour anomaly involving the measurement of the anomalous magnetic moment of the muon $(g-2)_\mu$ [6, 7]. The most recent prediction of this quantity in the SM [8] has a 4.2σ discrepancy from the experimental measurement [9, 10]. If we define Δa_μ as the experimental difference between the experimental measurement value a_μ^{exp} and the SM prediction a_μ^{SM}, we obtain

$$\Delta a_\mu = a_\mu^{\text{exp}} - a_\mu^{SM} \approx (251 \pm 59) \times 10^{-11}\,, \tag{6}$$

where the error results from a combination of the theoretical and experimental uncertainties. It is expected in the future that results from J-PARC [11] and Fermilab [12] will be able to reduce this experimental uncertainty.

The goal of this work is to solve the problems mentioned above while simultaneously providing an origin for a DM candidate. In a previous work [13] a model was proposed by extending the work [14] which added three new fields to the SM: an $SU(3)_c$ coloured scalar which is also an $SU(2)_L$ singlet, Φ_3, one $SU(2)_L$ singlet colourless scalar, Φ_2, and one $SU(2)_L$ doublet vectorlike fermion, χ, with $0, \pm 1$ electric charge. In this work we will discuss a new model where instead the scalars are $SU(2)_L$ doublets and the fermion is an $SU(2)_L$ singlet. We wish to understand what is the role played by the group representations in providing a simultaneous solution to the three problems. While the Yukawa Lagrangian has a similar structure, the scalar potential is different in the two cases. More importantly, in this new model the scalars will couple to gauge

bosons giving rise to the possibility of a change in DM related observables.

2. The Model

As mentioned before, In the previous work [13] a model was considered where three new fields were added to the SM:

- A colourless scalar ϕ_2;
- A coloured scalar ϕ_3;
- A vectorlike fermion χ which may have a charge 0 or ± 1.

In that work (model 5), the scalars were $SU(2)_L$ singlets while the fermion was an $SU(2)_L$ doublet. Our goal is to compare it to the scenario where scalars are $SU(2)_L$ doublets and the fermion is an $SU(2)_L$ singlet: this model will be called model 3. The complete set of quantum numbers is shown in tables 2 and 2 for models 3 and 5, respectively:

	$\boldsymbol{SU(3)_c}$	$\boldsymbol{SU(2)_L}$	$\boldsymbol{U(1)_Y}$
$\boldsymbol{\chi_R}$	1	1	-1
$\boldsymbol{\phi_2}$	1	2	1/2
$\boldsymbol{\phi_3}$	3	2	7/6

Table 1: Charge assignment of the new fields for model 3.

	$\boldsymbol{SU(3)_c}$	$\boldsymbol{SU(2)_L}$	$\boldsymbol{U(1)_Y}$
$\boldsymbol{\chi}$	1	2	$-1/2$
$\boldsymbol{\phi_2}$	1	1	0
$\boldsymbol{\phi_3}$	3	1	2/3

Table 2: Charge assignment of the new fields for model 5.

where all fields are odd under a Z_2 symmetry, meaning that the allowed terms in the potential are formed by field combinations where each field may only appear an even number of times (and the allowed terms have at most mass dimension 4). The Yukawa Lagrangean 7 connects the dark sector with the SM one and is necessary to explain the B anomalies via one-loop diagrams. The charge of the new particles is defined by the interaction

$$\mathcal{L}_{int}^{NP} = y_{Qi}\bar{Q}_{Li}\phi_3\chi_R + y_{Li}\bar{L}_{Li}\phi_2\chi + h.c.\,, \tag{7}$$

where y_{Qi} and y_{Li} are constants, Q_{Li} and L_{Li} are the SM left-handed doublets for quarks and leptons and χ_R is the right-handed component of the new fermion. Therefore, for model 3 we have

- A fermion singlet χ_R with charge -1;
- A coloured scalar doublet ϕ_3, with $\phi_3^T = \begin{bmatrix}\phi_q^{+2/3} & \phi_q^{+5/3}\end{bmatrix}$, where $\phi_3^{+2/3}$ and $\phi_3^{+5/3}$ are complex scalar fields with electric charge $+5/3$ and $+2/3$ respectively;
- A colourless scalar doublet ϕ_2, with $\phi_2^T = \begin{bmatrix}\phi_l^{+1} & \frac{S+iA}{\sqrt{2}}\end{bmatrix}$, where ϕ_2^{+1} is a complex scalar field with charge $+1$ and we separated the lower component of the doublet in its real and imaginary parts S and A, which are real scalar fields with no charge and opposite CP parities;

while for model 5 we obtain

- A fermion doublet χ, with $\chi^T = (\chi^0, \chi^-)$, where χ^0 and χ^- are complex fermionic fields with electric charge 0 and -1 respectively;
- A coloured scalar singlet $\phi_3^{+2/3}$ with electric charge $+2/3$;
- A colourless neutral scalar singlet ϕ_2, which can be separated in its real and imaginary part as $\phi_2 = (S + iA)/\sqrt{2}$.

The SM and DM sectors also interact via the scalar potential. In model 3, where the scalars are $SU(2)_L$ doublets, the scalar potential is given by (with all parameters real)

$$\begin{aligned} V(H,\phi_l,\phi_q) = &- m_{11}|\phi_1|^2 + m_{22}|\phi_2|^2 + m_{33}|\phi_3|^2 + \lambda_1|\phi_1|^4 + \lambda_2|\phi_2|^4 - \lambda_3|\phi_{3,a}|^2|\phi_{3,b}|^2 + \\ &+ \lambda_{12}|\phi_1|^2|\phi_2|^2 + \lambda_{13}|\phi_1|^2|\phi_3|^2 + \lambda_{23}|\phi_2|^2|\phi_3|^2 + \lambda_5[(\phi_1^\dagger\phi_2)^2 + (\phi_2^\dagger\phi_1)^2] \\ &+ \lambda'_{12}(\phi_1^\dagger\cdot\phi_2)(\phi_2^\dagger\cdot\phi_1) + \lambda'_{13}(\phi_1^\dagger\cdot\phi_3)(\phi_3^\dagger\cdot\phi_1) + \lambda'_{23}(\phi_2^\dagger\cdot\phi_3)(\phi_3^\dagger\cdot\phi_2)p \\ &+ y_{13}(\phi_3^\dagger\cdot\tau_2\cdot\phi_1)(\phi_1^\dagger\cdot\tau_2\cdot\phi_3) + y_{23}(\phi_3^\dagger\cdot\tau_2\cdot\phi_2)(\phi_2^\dagger\cdot\tau_2\cdot\phi_3)\,, \end{aligned} \tag{8}$$

where ϕ_1 is the usual Higgs field in unitary gauge $\phi_1^T \to \begin{bmatrix}0 & \frac{v_H+h}{\sqrt{2}}\end{bmatrix}$, with v being the vacuum expectation value (vev) $v \approx 246$ GeV and h the SM Higgs field. Furthermore, σ_2 is the second Pauli matrix. Note that usually the colour indices in ϕ_3 are omitted and a summation over colour is implied, except for the term proportional to λ_3 where the colour indices may be different. The remaining terms include the possibilities invariant under all symmetries when ϕ_3 is present.

Since only the SM-Higgs-Doublet acquires a vev, we obtain a minimization condition of $m_{11}^2 = v^2\lambda_1$ and thus the scalar potential has 15 free parameters. We chose as the free input parameters of the potential the masses of the scalar fields and the quartic parameters λ_2, λ_3, λ_{12}, λ_{13}, λ_{23}, λ'_{23}, y_{13} and y_{23} are fixed by the W mass. Therefore,

the following parameters were fixed

$$\lambda_1 = \frac{m_h^2}{2v^2} \qquad m_{22} = \frac{2m_{\phi_l}^2 - v^2\lambda_{12}}{2}\,,$$
$$\lambda_5 = \frac{m_S^2 - m_A^2}{2v^2} \qquad \lambda'_{12} = \frac{m_S^2 + m_A^2 - 2m_{\phi_l}^2}{v^2}\,,$$
$$m_{33}^2 = \frac{2m_{\phi_l^{+5/3}} - v^2 y_{13} - v^2\lambda_{13}}{2}\,,$$
$$\lambda'_{13} = \frac{2m_{\phi_q^{+2/3}} - 2m_{\phi_q^{+5/3}} + v^2 y_{13}}{v^2}\,,$$

where m_S, m_A, m_{ϕ_l} are the masses of the colourless scalars S, A and ϕ_l and $m_{\phi_q^{+5/3}}$, $m_{\phi_q^{+2/3}}$ are the masses of the coloured scalars $\phi_q^{+5/3}$, $\phi_q^{+2/3}$. Model 5 could have a fermionic candidate for DM. In model 3, the DM candidate can only be one of the neutral components of ϕ_2, either S or A, similarly to what was done on the previous work [13]. Since the two DM candidates are identical in terms of DM and flavor phenomenology, we may assume that $M_S < M_A$ so that S comprises the whole DM density. This condition implies that $\lambda_{10}\mu_1/\lambda_1 < 0$.

Moreover, the Dirac mass of the fermion χ is given by the Lagrangean term $m_\chi \bar{\chi_L}\chi_R + h.c.$ and the Yukawa interaction (7) can be rewritten as

$$\begin{aligned}\mathcal{L} =& y_{di}(\bar{u_{Lj}}V_{ji}\chi^-\phi_q^{+5/3} + \bar{d_{Li}}\chi^-\phi_q^{+2/3}) + \\ &+ y_{Li}\left(\bar{\nu_{Li}}\chi^-\phi_l^+ + \frac{e_{Li}}{\sqrt{2}}\chi^-(S+iA)\right) + h.c.\,,\end{aligned} \tag{9}$$

where y_{di} are the coupling constants for the quarks in their mass eigenstates and V is the Cabibbo-Kobayashi-Maskawa (CKM) matrix. For simplicity, we only take y_b, y_s and y_μ to be non-zero.

Finally, since we introduced new particles to the SM, for model 3 we must also introduce the electroweak oblique parameters S, T and U [15, 16], which are able to quantify deviations from the SM due to corrections on the two-point functions using electroweak data [17]. Therefore, one can write for the total two point function

$$\Pi_{ab}(q^2) = \Pi_{ab}^{SM}(q^2) + \delta\Pi_{ab}(q^2)\,, \tag{10}$$

where a, b can be one of the gauge bosons γ, Z and $W^\pm$, q^2 is the external squared momentum and $\delta\Pi_{ab}$ is the new physics contributions. In model 5, the contributions for these parameters is zero because both fields are $SU(2)_L$ singlets and the two components in the doublet fermion χ have the same mass, leading to a vanishing to the electroweak oblique parameters at one-loop level. In this work we only considered the limits on the parameter T. The fermion χ has a vanishing contribution to T (because the fermion vacuum polarization diagram at one-loop is zero in the limit where the momentum goes to zero, similarly to what happens in QED). Therefore, the only contributions for the T parameter come from the scalar fields. Following [18], we considered a general expression for the parameter T with an arbitrary number of scalar doublets with hypercharge $\pm 1/2$ and scalar singlets. In model 3, if we just consider ϕ_1 and ϕ_2, this corresponds to a 2HDM with a dark doublet [19] where the NP contribution is given by [18]:

$$T = \frac{g^2}{64\pi^2 M_W^2 \alpha}[F(M_{\phi_l}^2, M_S^2) + F(M_{\phi_l}^2, M_A^2) - F(M_S^2, M_A^2)]\,, \tag{11}$$

where m_W is the mass of the $W^\pm$ gauge boson, α is the fine structure constant and g is the $SU(2)_L$ coupling constant. The function $F(A, B)$ is given by

$$F(A,B) = \begin{cases} \frac{A+B}{2} - \frac{AB}{A-B}\log\frac{A}{B} & , A \neq B \\ 0 & , A = B \end{cases}. \tag{12}$$

Similarly for ϕ_3, one can prove that the T parameter is proportional to $F(m_{\phi_{qu}}^2, m_{\phi_{qd}}^2)$ and thus vanishes, since the masses of these scalars are set to be equal. Therefore, the T parameter contribution only comes from the expression (11), with the limit being used $T = 0.03 \pm 0.12$, which will be applied at the end of the scan.

3. Phenomenology

In this section we discuss the flavour constraints of the model. We must verify that not only we solve the discrepancies observed experimentally but also make sure that the observables in agreement with the SM predictions are not modified. Since the phenomenology is identical for both models, that is, both model 3 and model 5 have the same NP contributions to the relevant flavour observables, then we can use the same constraints and analytic expressions as in [13] for both models.

3.1. Anomalous moment of the muon $(\mathbf{g-2})_\mu$

We start by analysing the anomalous magnetic moment of the muon. In model 3, the leading order (LO) NP contribution comes from one-loop diagrams containing the fermion χ and the scalars S or A and we can write [20]

$$\Delta a_\mu = \frac{m_\mu^2 |y_\mu|^2}{16\pi^2}[\tilde{F}_7(x_S) + \tilde{F}_7(x_A)]\,, \tag{13}$$

with

$$\tilde{F}_7(x) = \frac{1 - 6x + 3x^2 + 2x^3 - 6x^2 Lnx}{12(1-x)^4} \tag{14}$$

and $x_{S(A)} = m_{S(A)}^2/m_\chi^2$.

3.2. $\mathbf{B \to K^* \mu^+ \mu^-}$ decay

The effects of the loop transition $b \to s\mu^+\mu^-$ illustrated in figure 1 can be described using an effective field theory. For that, we generate an effective Hamiltonian for this new interaction given by [21, 22]

$$\mathcal{H}_{eff} = -\frac{4G_F}{\sqrt{2}} V_{tb}V_{ts}^*(C_9^{NP}\mathcal{O}_9 + C_{10}^{NP}\mathcal{O}_{10})\,, \tag{15}$$

where V_{tb} and V_{ts}^* are CKM matrix elements, C_9^{NP} and C_{10}^{NP} are the Wilson coefficients and $\mathcal{O}_9$, $\mathcal{O}_{10}$ are the following operators:

$$\mathcal{O}_9 = \frac{\alpha}{4\pi}[\bar{s}\gamma^\nu P_L b][\bar{\mu}\gamma_\nu \mu] \tag{16}$$
$$\mathcal{O}_{10} = \frac{\alpha}{4\pi}[\bar{s}\gamma^\nu P_L b][\bar{\mu}\gamma_\nu\gamma_5 \mu]\,. \tag{17}$$

The main contribution to these operators comes from the box diagram in figure 1 and the respective Wilson coefficients are given by [20, 13]

$$C_9^{box} = -C_{10}^{box} = \mathcal{N}\frac{y_s y_b^* |y_\mu|^2}{64\pi\alpha m_\chi^2}[F(x_{\phi_q}, x_S) + F(x_{\phi_q}, x_A)]\,, \tag{18}$$

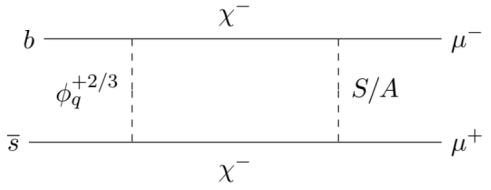

Figure 1: One-loop Feynman diagram to solve the $R(K^{(*)})$ anomalies.

with $\mathcal{N}^{-1} = \frac{4G_F V_{tb} V_{ts}^*}{\sqrt{2}}$, $x_{\phi_q,S,A} = \frac{m^2_{\phi_q,S,A}}{m^2_\chi}$ and

$$F(x,y) = \frac{1}{(1-x)(1-y)} + \frac{x^2 lnx}{(1-x)^2(x-y)} + \frac{y^2 lny}{(1-y)^2(y-x)} \,. \tag{19}$$

Considering the most recent experimental results, the best fitted values of the Wilson coefficients are $C_9^{NP} = -C_{10}^{NP} = [-0.59, -0.30]$ [23], with a 2σ confidence level and therefore in our scan we will consider the points in the parameter space that generate values of C_9^{NP} within the 2σ range of its central value.

3.3. $\mathbf{B_s - \bar{B}_s}$ mixing

Another relevant constraint associated to the $b \to s$ transition comes from the $B_s - \bar{B}_s$ mixing, which consists on the phenomena where the B_s meson oscillates between its particle and antiparticle. Here, the only contribution arises from the effective operator

$$\mathcal{H}_{eff}^{B\bar{B}} = C_{B\bar{B}} (\bar{s_\alpha} \gamma^\mu P_L b_\alpha)(\bar{s_\beta} \gamma^\mu P_L b_\beta) \,, \tag{20}$$

where α and β denote the coloured indices. The NP contribution to the Wilson coefficient is given by [20]

$$C_{B\bar{B}}^{NP} = \frac{(y_s y_b^*)^2}{128\pi^2 m_\chi^2} F(x_{\phi_q}, x_{\phi_q}) \,, \tag{21}$$

with

$$F(x,x) = \frac{1 - x^2 + 2x lnx}{(1-x)^3} \,. \tag{22}$$

The constraint is set on the mass difference ΔM_s of the two states B_s and $\bar{B}_s$. We can represent this constraint in terms of the ratio of the experimental and SM values for the mass difference, defining the quantity [24]:

$$R_{\Delta M_s} = \frac{\Delta M_s^{exp}}{\Delta M_s^{SM}} - 1 = -0.09 \pm 0.08 \quad at\ 1\sigma\ C.L.. \tag{23}$$

One can thus write $R_{\Delta M_s}^{exp}$ in terms of the NP and SM Wilson coefficients [24, 25]:

$$R_{\Delta M_s} = \left| 1 + \frac{0.8 C_{B\bar{B}}^{NP}(\mu_H)}{C_{B\bar{B}}^{SM}} (\mu_b) \right| - 1 \,, \tag{24}$$

with $C_{B\bar{B}}^{NP}(\mu_H)$ being the NP Wilson coefficient at $\mu_H = 1TeV$ and $C_{B\bar{B}}^{SM}(\mu_b) \approx 7.2 \times 10^{-11} GeV^{-2}$ the corresponding SM value at the scale μ_b [26].

4. Dark Matter phenomenology

In this section we discuss the constraints arising from DM physics, taking into account DM relic density observations, constraints from DM direct detection and collider searches. The particle S is the chosen DM candidate. However, choosing A would lead to identical results since both particles have identical quantum numbers. Since S is a DM candidate, it must be able to reproduce the current DM relic abundance $\Omega_{DM} h^2 = 0.1199 \pm 0.0022$ [27]. We assume that the DM relic density is originated by a freeze-out mechanism and thus the number density of S n_S can be obtained through the Boltzmann equation

$$\frac{dn_S}{dt} + 3Hn_S = -\langle \sigma v \rangle \left(n_S^2 - n_{S_{eq}}^2 \right) , \tag{25}$$

where $n_{S_{eq}}$ is the number density of S at equilibrium, H is the Hubble parameter and $\langle \sigma v \rangle$ is the thermally averaged DM annihilation cross section times its relative velocity. The Boltzmann equation (25) can be solved numerically using the software MICROMEGAS [28] which takes into account all possible DM annihilation and co-annihilation channels. The freeze-in mechanism, which is also a well-known alternative mechanism that explains DM abundance cannot be used in this case since our model requires very weak couplings between the DM particle and the visible sector $\mathcal{O}(10^{-10} - 10^{-12})$ [29].

An interesting aspect of model 3 is that, since the scalar fields are doublets, they can couple to the gauge bosons, unlike model 5 where the scalar fields are singlets. This will drastically change the distribution of the DM relic abundance. The relevant annihilation and co-annihilation processes are present in figures 2, 3 for model 3 and 4, 5 for model 5:

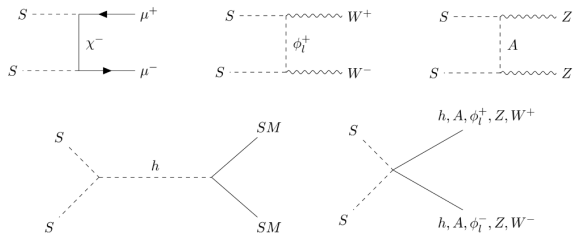

Figure 2: Diagrams for DM Annihilation in model 3; SM represents all SM massive particles.

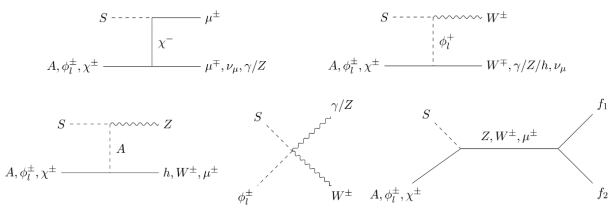

Figure 3: Diagrams for DM Co-annihilation in model 3; f_1, f_2 represent all possible SM final states of the s diagram.

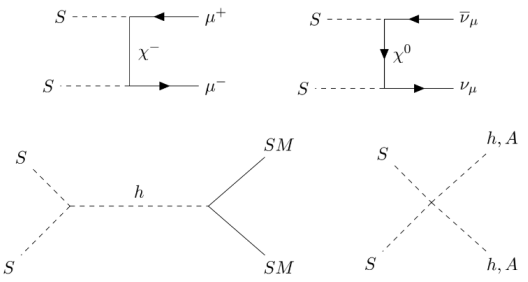

Figure 4: Diagrams for DM Annihilation in model 3; SM represents all SM massive particles.

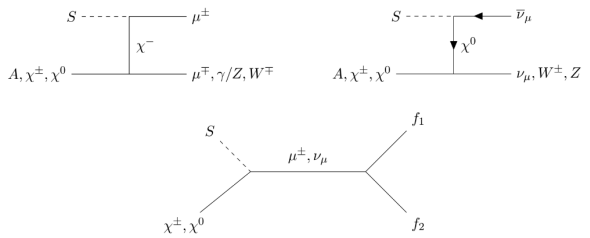

Figure 5: Diagrams for DM Co-annihilation in model 3; f_1, f_2 represent all possible SM final states of the s diagram.

Besides the relic density constraint, we must take into account DM direct detection (DD) results which may also place several constraints on the parameter space of model 3. Currently, the best experimental upper bounds on the DM direct detection cross section for a mass above 6 GeV are provided by the PandaX-4T [30] and the XENON1T [31] experiments. We will show the three limits in our plots which will allow to understand the effect of future DD bounds. In model 3, the dominant DM DD channel is a tree-level t-channel with a Higgs-like mediation corresponding to the scattering process $SN \to SN$ (with N representing a nucleon), which has a cross section

$$\sigma(SN \to SN) = \frac{(\lambda_{12} + \lambda'_{12} + 2\lambda_5)^2}{4\pi} \frac{f_N^2 m_N^2 \mu_{SN}^2}{m_S^2 m_h^4}\,, \quad (26)$$

where $f_N \approx 0.3$ is an effective Higgs-nucleon coupling, m_N is the nucleon mass and μ_{SN} is the DM-nucleon reduced mass [32, 33, 34, 35].

Another source of constraints to the model is the result of collider searches on DM at LHC, in particular the constraint of a SM-Higgs boson decaying into an S pair. For this decay, which is allowed when $m_S < m_h/2$, the width is given by

$$\Gamma(h \to SS) = \frac{(\lambda_{12} + \lambda'_{12} + 2\lambda_5)^2 v^2}{32\pi m_h} \sqrt{1 - \frac{4m_S^2}{m_h^2}} \quad (27)$$

and currently has an upper bound of 0.11 [36]. These are the DM searches constraints considered in this study. As we will see, the DM DD limit gives rise to a much stricter limit than the Higgs invisible width.

5. Results

5.1. Initial scan setup

In this section, we discuss the results obtained for model 3 by performing a multi parameter scan taking into account the flavour and DM constraints mentioned before, in order to obtain the allowed parameter space for the model. The relevant parameters for Model 3 are

$$y_b, y_s, y_\mu, m_\chi, m_{\phi_q^{+5/3}}, m_{\phi_q^{+2/3}}, m_S, m_A, m_{\phi_l}, \lambda_{hS}, \lambda_2\,,$$

with $\lambda_{hS} = \lambda_{12} + \lambda'_{12} + 2\lambda_5$ being the Higgs portal coupling. It would be expected that the quartic parameters λ_{23}, λ'_{23} and y_{23} were also relevant, since they have an impact in the DM abundance through co-annihilation channels involving the coloured scalar fields. However, since there is a huge difference between the DM mass and masses of the coloured scalars, the contribution of these processes to the relic density will be very small. The values chosen for these parameters were $\lambda_{23} = \lambda'_{23} = y_{23} = 10^{-3}$. The parameters λ_3, λ_{13} and y_{13} are irrelevant for the discussion since they have no contribution for the DM and flavour physics.

The results are divided in two scans: In scan I (figures 6 and 7) our goal was to get a feel for the allowed parameter space of model 3 by varying its input parameters, while in scan II we fine-tuned the parameters taking into account the results from scan I in order to find points that satisfy all previously mentioned constraints. Therefore, the results from scan II are our final results. It is necessary to explain the meaning of each color of the points present in our figures: all points in the parameter space explain the B meson data within a 2σ confidence interval. The blue points furthermore explain the DM relic density value, the green points also satisfy XENON1T DM DD and collider searches constraints and the red points additionally satisfy the muon $(g-2)$ data within 3σ (that is, all constraints simultaneously).

Before analysing the results, we need to discuss some simplifications made and the allowed values considered for the parameter scan: following the reasoning of [13], in the flavour phenomenology expressions of the B meson decay and $B_s - \bar{B}_s$ mixing, the coupling constants y_s and y_b appear exclusively in the combination $y_s y_b^*$ and therefore one may assume they are real and proportional to each other, with $y_s = -y_b/4$. The minus sign appears because the product must be negative in order to solve the measurements of $R(K)$. Moreover we set $|y_b| \leq 1$ for both scans, $0 \leq y_\mu \leq 4\pi$ (scan I) and $1 \leq y_\mu \leq 4\pi$ (scan II), where the condition $1 \leq y_\mu$ appears for optimization purposes. We also fix the masses of the coloured scalars at 1.5 TeV, similarly to model 5, and force all other dark sector particles to be heavier than the DM candidate S by at least 10 GeV (and at most 1 TeV) in both scans, considering 5 GeV$\leq M_S \leq$ 1 TeV (scan I) which is the average WIMP mass range, and 5 GeV$\leq M_S \leq$ 100 GeV (scan II), where the upper limit $m_S \leq 100$ GeV appears to optimize the scan, since for reasons we will explain ahead m_S is restricted to be below 80 GeV to satisfy the DM constraints. For the masses of the remaining scalars, we take 15 GeV$\leq m_A, m_{\phi_l} \leq$ 2 TeV (scan I). In scan II however, we consider constraints from the precision data and LEP experiments of the W and Z boson widths. Additionally, for the decays $W^\pm \to S\phi_l^\pm, A\phi_l^\pm$ and $Z \to SA, \phi_l^+\phi_l^-$ to be kinematically forbidden, the following relations must be verified

$$m_S + m_{\phi_l} > m_W \qquad m_A + m_{\phi_l} > m_W \quad (28)$$
$$m_S + m_A > m_Z \qquad 2m_{\phi_l} > M m_Z\,. \quad (29)$$

Moreover, the process $e^+e^- \to \phi_l^+\phi_l^-$ also sets the limit $m_{\phi_l} > 70$ GeV [37]. We also exclude the region where simultaneously $m_S < 80$ GeV, $m_A < 100$ GeV and $m_A - m_S > 8$ GeV, since they would allow a visible di-jet or di-lepton signal [38]. Thus we have 100 GeV$\leq m_A \leq 1.1$ TeV and 70 GeV$\leq m_{\phi_l} \leq 1.1$ TeV in scan II. We also imposed $m_A \geq 100$ GeV since in scan I we concluded that $m_S \leq 80$ GeV (and $m_A - m_S > 8$ GeV is immediately satisfied by design). Furthermore, the masses m_S, m_A and m_{ϕ_l} should be such that λ'_{12} and λ_5 are smaller than the perturbative limit 4π (in both scans). For the vectorlike fermion χ, we set the lower limit 101.2 GeV$\leq m_\chi \leq 2$ TeV (scan I) and 101.2 GeV$\leq m_\chi \leq 1.1$ TeV (scan II), where the lower limit comes from LEP searches for unstable heavy vectorlike charged leptons [39]. More recent constraints from the LHC exist for vectorlike leptons, but they do not apply to our model since those searches assume that the vectorlike leptons couple to tau leptons [40], or have very small amounts of missing transverse energy, $\not{E}_T$, in the final states [41]. Regarding the Higgs portal coupling, we impose $|\lambda_{hS}| \leq 1$ (scan I), which is achieved by setting $10^{-5} \leq \lambda_{12} \leq 0.5$ and rejecting points where $\lambda_5 < -0.2$ and $|\lambda'_{12}| \geq 0.1$.

As for scan II, we used $10^{-7} \leq |\lambda_{hS}| \leq 10^{-2}$, and $\lambda_{12}, |\lambda_5|, |\lambda'_{12}| \leq 4\pi$. Unlike in model 5 where the Higgs portal coupling is a completely free parameter, here it depends on the masses of S and ϕ_l and thus needs to be fine-tuned in order to be very small (this will be discussed in more detail ahead). Finally, we consider λ_2, whose only contribution is to the DM relic density through the channels $SS \to AA, \phi_l^+\phi_l^-$. We take $\lambda_2 = 10^{-5}$ in order to suppress the channel contribution to the relic abundance. A summary of the values used for each parameter in scans I and II is shown in Tables 3 and 4, respectively:

y_b	y_s	y_μ	$m_\chi(GeV)$	$m_{\phi_q^{+5/3}}, m_{\phi_q^{+2/3}}(GeV)$
$[-1, 1]$	$-y_b/4$	$1, 4\pi$	$[101.2, 1100]$	1500
$m_S(GeV)$	$m_A(GeV)$	$m_{\phi_l}(GeV)$	λ_{12}	λ_2
$[5, 1000]$	$[15, 2000]$	$[15, 2000]$	$[10^{-5}, 0.5]$	10^{-5}

Table 3: Input values for model 3 scan I. Additionally, we impose $|\lambda_{hS}| \leq 1$, which is achieved by considering $\lambda_5 < -0.2$ and $|\lambda'_{12}| \geq 0.1$.

y_b	y_s	y_μ	$m_\chi(GeV)$	$m_{\phi_q^{+5/3}}, m_{\phi_q^{+2/3}}(GeV)$
$[-1, 1]$	$-y_b/4$	$1, 4\pi$	$[101.2, 1100]$	1500
$m_S(GeV)$	$m_A(GeV)$	$m_{\phi_l}(GeV)$	λ_{12}	λ_2
$[5, 100]$	$[100, 1100]$	$[70, 1100]$	$\leq 4\pi$	10^{-5}

Table 4: Input values for model 3 scan II. Additionally, we impose $10^{-7} \leq |\lambda_{hS}| \leq 10^{-2}$, which is achieved by considering $\lambda_5, |\lambda'_{12}| \leq 4\pi$.

5.2. **Model parameter space**

In both models it was possible to find a region of the parameter space which satisfies all constraints. However, this region is different for both models, with the main difference being related to the DM relic density as a function of its mass, as it can be observed in figure 6:

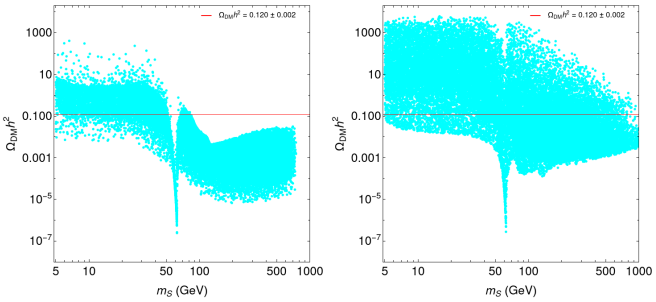

Figure 6: Scan I - DM relic density as a function of the DM mass for model 3 (left) and model 5 (right). The cyan points satisfy the B meson anomalies within a 2σ confidence value. The red line represents the observed DM relic density. For model 3, we also take $|\lambda_4| \leq 0.2$, $|\lambda_7| \leq 0.1$ and $|\lambda_{10}| \leq 0.5$. For model 5, the parameter values are the ones used in [13].

We immediately identify the same lower peak on both figures, around 60 GeV, which corresponds to the region of SM Higgs resonance $m_S \approx m_h/2$. In model 3, the DM mass has an upper limit of 80 GeV, while for model 5 no limit is observed. This result can be easily explained since the scalar fields in model 3 and model 5 have different $SU(2)_L$ representations: in model 5 the scalar fields are singlets while in model 3 they are doublets and allowed to couple to gauge bosons. Therefore, in model 3 the DM annihilation processes $SS \to W^+W^-$ and $SS \to ZZ$ are allowed, which does not happen in model 5. Thus in model 3 the DM relic density is smaller than the value given by the Planck observation when $m_S \geq m_W$, similarly to what was observed for the i2HDM [42]. Another distinction between the models comes from the Higgs portal coupling: while in model 5 the λ_{hS} parameter can be as small as desired, in model 3 one has the relation

$$\lambda_{hS} = \lambda_{12} + \lambda'_{12} + 2\lambda_5 = \lambda_{12} + 2\frac{(M_S^2 - M_{\phi_l}^2)}{v^2}\,. \qquad (30)$$

Therefore, to have small values of λ_{hS} (of $\mathcal{O}(10^{-2})$), which is a constraint required by the experimental upper bounds of the LZ, PandaX-4T and XENON1T experiment, the difference between the masses of S and ϕ_l must be small or else we must verify that λ_{12} is very close to $-2(m_S^2 - m_{\phi_l}^2)/v^2$. This condition is shown in figure 7:

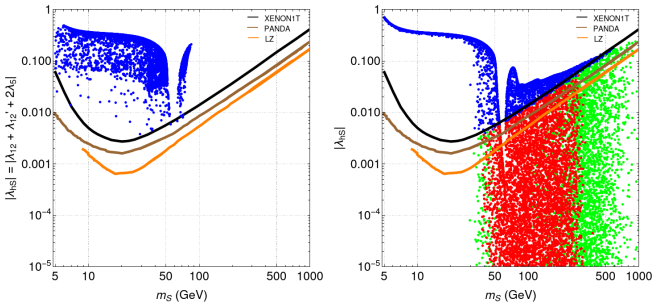

Figure 7: Scan I - Higgs portal coupling $|\lambda_{HSS}|$ as a function of the DM mass. The solid black, brown and orange lines represent an experimental upper bound provided by the XENON1T, PANDAX-4T and LZ experiments respectively. The values used for the parameters in the models are the same as in figure 6.

As opposed to what we see in model 5, all points in

model 3 are excluded due to DM DD and Higgs decay constraints. Since m_S varies between $[5, 1000]$ GeV and the minimum mass difference between S and other new particle is 10 GeV, then the quantity $\left|2\left(m_S^2 - m_{\phi_l}^2\right)/v^2\right|$ can only be as small as ≈ 0.0066 and therefore the condition $\lambda_{hS} \leq 10^{-2}$ is extremely unlikely to occur without forcing $\lambda_{12} \approx -2\left(m_S^2 - m_{\phi_l}^2\right)/v^2$ or $m_S - m_{\phi_l}$ to be smaller. We chose to keep λ_{hS} small since the other option would make the co-annihilation processes more efficient and affect the DM relic density. The main results for model 3 are present in figures 8, 9 and 10 (scan II):

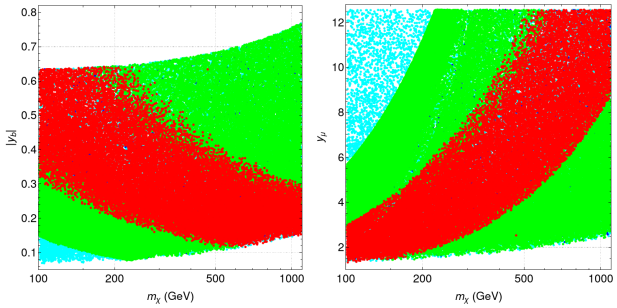

Figure 8: Scan II - Model 3 parameter space for $(|y_b|, M_\chi)$(left) and (y_μ, m_χ)(right) considering the parameter values $1 \leq y_\mu \leq 4\pi$, $10^{-7} \leq |\lambda_{HSS}| \leq 10^{-2}$ and $|\lambda_4|, |\lambda_7|, |\lambda_{10}| \leq 4\pi$.

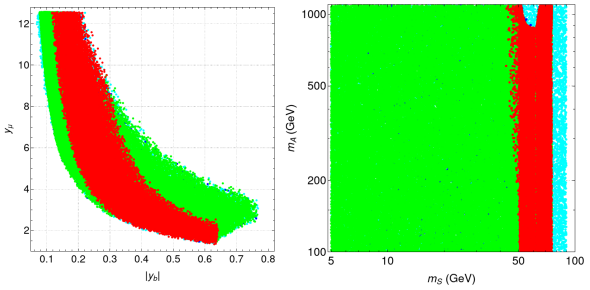

Figure 9: Scan II - Model 3 parameter space for $(y_\mu, |y_b|)$(left) and (m_A, m_S)(right).

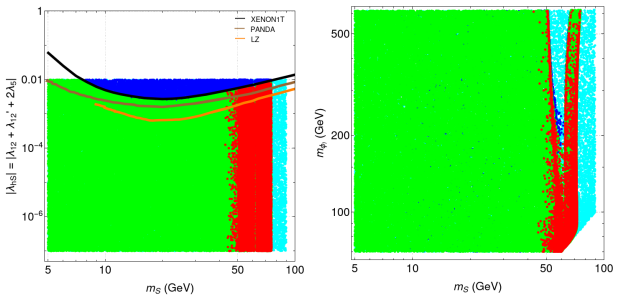

Figure 10: Scan II - Model 3 parameter space for $(|\lambda_{HSS}|, m_S)$(left) and (m_{ϕ_l}, m_S)(right). The solid black, brown and orange lines represent an experimental upper bound provided by the XENON1T, PANDAX-4T and LZ experiments respectively.

We see that the obtained results for the Yukawa couplings are similar to the ones in model 5, which was already expected since the flavour physics in both models is the same and the DM constraint do not have a big impact in the parameter space of these values. We obtained $|y_\mu| > 1.3$ and $0.11 \leq |y_b| \leq 0.65$ when all constraints are satisfied. We also note that, as we already saw in figure 6, the DM relic density limits the allowed value for the DM mass at $m_S < 80$ GeV. By further taking into account the $(g-2)$ constraint, we obtain 42 GeV$< m_S <$ 76 GeV, whereas in model 5 the allowed mass range was 30 GeV$< m_S <$ 350 GeV. This is a significant change in the allowed parameter space of the models: in model 3 the DM mass is limited in a very narrow range, while for model 5 the range is much wider. For the remaining parameters, we can observe in figure 9 that $M_A < 1076$ GeV. In figure 10, we present the bounds from the XENON1T, PandaX-4T and LZ and conclude that $m_{\phi_l} < 621$ GeV. The lower limit on m_{ϕ_l} was already expected since it is necessary to keep $\lambda_{12} < 4\pi$.

Afterwards, we applied the oblique T parameter to the allowed parameter space and obtained the following results, within a 2σ confidence value for the T parameter experimental bound:

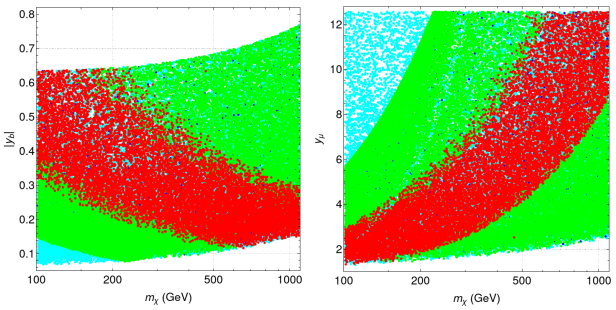

Figure 11: Model 3 parameter space for $(|y_b|, M_\chi)$(left) and (y_μ, M_χ)(right) after applying the T parameter limit.

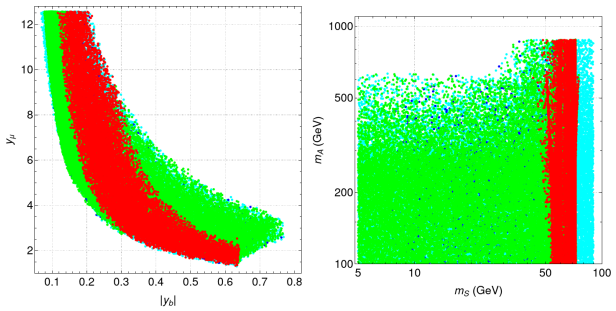

Figure 12: Model 3 parameter space for $(y_\mu, |y_b|)$(left) and (M_A, M_S)(right) after applying the T parameter limit.

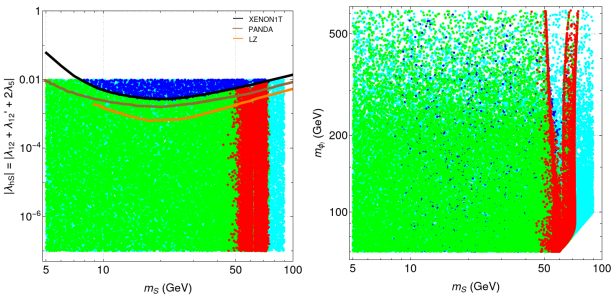

Figure 13: Model 3 parameter space for (λ_{HSS}, M_S)(left) and (M_{ϕ_l}, M_S)(right) after applying the T parameter limit.

We observe two major changes: the maximum allowed

mass for A goes from 1076 GeV to 877 GeV, and for heavier masses ($m_{\phi_l} > 200$ GeV and $m_A > 300$ GeV), the vast majority of the allowed parameter space is now excluded. This is shown on figure 14, where now all points satisfy all previously mentioned constraints:

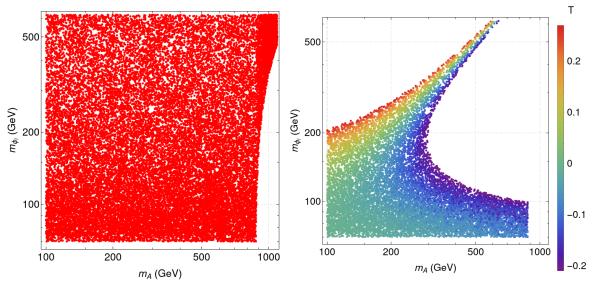

Figure 14: Model 3 parameter space for (M_{ϕ_l}, M_A) before applying the oblique parameter T limit(left) and after(right); The points presented here satisfy all constraints. The point color scheme on the right image describes different values for the T parameter.

As one can see on the right image in figure 14, the effects of the T parameter is to select regions close to the limit $m_{\phi_l} \approx m_A$, since this leads to $T \approx 0$. This is particularly true for large mass values $m_{\phi_l} > 200$ GeV. However, one can make the approximation $T \propto (m_{\phi_l} - m_A)/(m_{\phi_l} - m_S)$ [43] and thus significant mass splits can still be observed for small values of m_{ϕ_l}, where $m_{\phi_l} \approx m_S$. For larger values of M_{ϕ_l}, the only way to keep T in its experimental bound is to have $M_A \approx M_{\phi_l}$, which excludes a significant part of the parameter space in this region. Although only the T parameter was considered, the S parameter is not expected to affect greatly the model, since it only has a logarithmic dependence on the mass split [43, 42].

6. Conclusions

We studied a model which provides a solution to the SM problem of lepton universality flavour violation in the $b \to s\mu^+\mu^-$ decay brought up by the LHCb and Belle collaborations. Additionally, this model also solves the muon $(g-2)$ anomaly and provides a DM candidate. In a previous work [13], a similar model was studied which differs from the present work in the group representation of the new dark sector scalar and fermion fields: in the previous model, the vector-like fermion χ was an $SU(2)_L$ doublet while the complex scalar fields ϕ_l and ϕ_q were $SU(2)_L$ singlets, with ϕ_q being an $SU(3)_c$ triplet. In this model, χ is an $SU(2)_L$ singlet while ϕ_l and ϕ_q are doublets.

We wanted to analyse how the different group representations affect the allowed parameter space of the models. The Yukawa Lagrangean for both models is such that the vertices present in the loop process which provides the NP results are identical, meaning that the contributions to the flavour observables and $(g-2)$ are the same. However, there are two major differences related to the DM observables: first, in order to explain the DM relic density value obtained by the Planck Collaboration, the DM mass must be lower than 80 GeV for model 3, whereas in model 5, this restriction does not exist. This is due to the fact that in model 3, the DM scalar field can couple to the gauge bosons, which allows the annihilation processes $SS \to W^+W^-$ and $SS \to ZZ$ to occur, leading to a small relic density contribution. Second, there is a huge difference regarding the Higgs portal coupling. While in Model 5 this parameter is free, in Model 3 it is constrained and written as $\lambda_{HSS} = \lambda_{12} + 2(M_S^2 - M_{\phi_l}^2)/v^2$. To obtain a small constant, one must either choose λ_{12} and $2(M_S^2 - M_{\phi_l}^2)/v^2$ to be simultaneously small or $\lambda_{12} \approx -2(M_S^2 - M_{\phi_l}^2)/v^2$, with the latter one being the most viable option and the portal coupling values allowed to vary between 10^{-7} and 10^{-2}. The constraints coming from μ related experiments are expected to be weak for both models but could affect the parameter space for points close to the perturbative limit $y_\mu \approx 4\pi$.

In conclusion, the DM constraints are the ones acting on the models in a dramatically different manner. This difference is shown in the DM allowed mass range: while for model 5 the mass range was 30 GeV$< m_S <$ 350 GeV, here in model 3 the range is more restricted at 42 GeV$< M_S <$ 76 GeV. Over the last year, two new bounds from the DM direct detection experiments PANDAX-4T and LZ were released [44, 45]. Although by taking this into account the value of the portal coupling constant decreased, there were no changes on the allowed DM mass range.

References

[1] Roel Aaij et al. Test of lepton universality in beauty-quark decays. *Nature Phys.*, 18(3):277–282, 2022.

[2] Roel Aaij et al. Search for lepton-universality violation in $B^+ \to K^+\ell^+\ell^-$ decays. *Phys. Rev. Lett.*, 122(19):191801, 2019.

[3] R. Aaij et al. Test of lepton universality with $B^0 \to K^{*0}\ell^+\ell^-$ decays. *JHEP*, 08:055, 2017.

[4] Gudrun Hiller and Frank Kruger. More model-independent analysis of $b \to s$ processes. *Phys. Rev. D*, 69:074020, 2004.

[5] Marzia Bordone, Gino Isidori, and Andrea Pattori. On the Standard Model predictions for R_K and R_{K^*}. *Eur. Phys. J. C*, 76(8):440, 2016.

[6] M. Tanabashi et al. Review of Particle Physics. *Phys. Rev. D*, 98(3):030001, 2018.

[7] T. P. Gorringe and D. W. Hertzog. Precision Muon Physics. *Prog. Part. Nucl. Phys.*, 84:73–123, 2015.

[8] T. Aoyama et al. The anomalous magnetic moment of the muon in the Standard Model. *Phys. Rept.*, 887:1–166, 2020.

[9] B. Abi and Albahri et. al. Measurement of the positive muon anomalous magnetic moment to 0.46 ppm. *Phys. Rev. Lett.*, 126:141801, Apr 2021.

[10] G. W. Bennett et al. Final Report of the Muon E821 Anomalous Magnetic Moment Measurement at BNL. *Phys. Rev. D*, 73:072003, 2006.

[11] Naohito Saito. A novel precision measurement of muon g-2 and EDM at J-PARC. *AIP Conf. Proc.*, 1467:45–56, 2012.

[12] J. Grange et al. Muon (g-2) Technical Design Report. 1 2015.

[13] Da Huang, António P. Morais, and Rui Santos. Anomalies in b-meson decays and the muon $g-2$ from dark loops. *Phys. Rev. D*, 102:075009, Oct 2020.

[14] D. G. Cerdeño, A. Cheek, P. Martín-Ramiro, and J. M. Moreno. B anomalies and dark matter: a complex connection. *Eur. Phys. J. C*, 79(6):517, 2019.

[15] Michael E. Peskin and Tatsu Takeuchi. New constraint on a strongly interacting higgs sector. *Phys. Rev. Lett.*, 65:964–967, Aug 1990.

[16] Michael E. Peskin and Tatsu Takeuchi. Estimation of oblique electroweak corrections. *Phys. Rev. D*, 46:381–409, Jul 1992.

[17] Gerhardt Funk, Deva O'Neil, and R. Michael Winters. What the Oblique Parameters S, T, and U and Their Extensions Reveal About the 2HDM: A Numerical Analysis. *Int. J. Mod. Phys. A*, 27:1250021, 2012.

[18] W Grimus, L Lavoura, O M Ogreid, and P Osland. A precision constraint on multi-higgs-doublet models. *Journal of Physics G: Nuclear and Particle Physics*, 35(7):075001, May 2008.

[19] Ernest Ma. Verifiable radiative seesaw mechanism of neutrino mass and dark matter. *Phys. Rev. D*, 73:077301, 2006.

[20] Pere Arnan, Lars Hofer, Federico Mescia, and Andreas Crivellin. Loop effects of heavy new scalars and fermions in $b \to s\mu^+\mu^-$. *JHEP*, 04:043, 2017.

[21] Wolfgang Altmannshofer, Patricia Ball, Aoife Bharucha, Andrzej J Buras, David M Straub, and Michael Wick. Symmetries and asymmetries of $b \to k\mu^+\mu^-$ decays in the standard model and beyond. *Journal of High Energy Physics*, 2009(01):019–019, jan 2009.

[22] Elia et. al Schneider. Complementarity of the constraints on new physics from $B_s \to \mu^+\mu^-$ and from $b \to k\ell^+\ell^-$ decays. *Phys. Rev. D*, 86:034034, Aug 2012.

[23] Marcel Algueró, Bernat Capdevila, Sébastien Descotes-Genon, Joaquim Matias, and Martín Novoa-Brunet. $b \to s\ell^+\ell^-$ global fits after R_{K_S} and $R_{K^{*+}}$. *Eur. Phys. J. C*, 82(4):326, 2022.

[24] Pere Arnan, Andreas Crivellin, Marco Fedele, and Federico Mescia. Generic loop effects of new scalars and fermions in $b \to s\ell^+\ell^-$, $(g-2)_\mu$ and a vector-like 4^{th} generation, 2021.

[25] F. Gabbiani, E. Gabrielli, A. Masiero, and L. Silvestrini. A complete analysis of fcnc and cp constraints in general susy extensions of the standard model. *Nuclear Physics B*, 477(2):321–352, 1996.

[26] A. Bazavov and Bernard et. al. $B^0_{(s)}$-mixing matrix elements from lattice qcd for the standard model and beyond. *Phys. Rev. D*, 93:113016, Jun 2016.

[27] Planck Collaboration and Aghanim, N.and Fernandez-Cobos, R. et. al. Planck 2018 results - vi. cosmological parameters. *A&A*, 641:A6, 2020.

[28] Genevieve Belanger, Ali Mjallal, and Alexander Pukhov. Recasting direct detection limits within micrOMEGAs and implication for non-standard Dark Matter scenarios. *Eur. Phys. J. C*, 81(3):239, 2021.

[29] G. Bélanger, F. Boudjema, A. Goudelis, A. Pukhov, and B. Zaldívar. micromegas5.0: Freeze-in. *Computer Physics Communications*, 231:173–186, Oct 2018.

[30] Yue Meng et al. Dark Matter Search Results from the PandaX-4T Commissioning Run. *Phys. Rev. Lett.*, 127(26):261802, 2021.

[31] E. Aprile and Aalbers et. al. Dark matter search results from a one ton-year exposure of xenon1t. *Phys. Rev. Lett.*, 121:111302, Sep 2018.

[32] James M. Cline, Pat Scott, Kimmo Kainulainen, and Christoph Weniger. Update on scalar singlet dark matter. *Phys. Rev. D*, 88:055025, Sep 2013.

[33] J. M. Alarcón, J. Martin Camalich, and J. A. Oller. Chiral representation of the πn scattering amplitude and the pion-nucleon sigma term. *Phys. Rev. D*, 85:051503, Mar 2012.

[34] Xiu-Lei Ren, Xi-Zhe Ling, and Li-Sheng Geng. Pion–nucleon sigma term revisited in covariant baryon chiral perturbation theory. *Physics Letters B*, 783:7–12, 2018.

[35] Martin Hoferichter, Philipp Klos, Javier Menéndez, and Achim Schwenk. Improved limits for Higgs-portal dark matter from LHC searches. *Phys. Rev. Lett.*, 119(18):181803, 2017.

[36] P.A. Zyla et al. Review of Particle Physics. *PTEP*, 2020(8):083C01, 2020. and 2021 update.

[37] Aaron Pierce and Jesse Thaler. Natural dark matter from an unnatural higgs boson and new colored particles at the TeV scale. *Journal of High Energy Physics*, 2007(08):026–026, aug 2007.

[38] Erik Lundstrom, Michael Gustafsson, and Joakim Edsjo. The Inert Doublet Model and LEP II Limits. *Phys. Rev. D*, 79:035013, 2009.

[39] P. Achard et. al. Search for heavy neutral and charged leptons in e+e annihilation at lep. *Physics Letters B*, 517(1):75–85, 2001.

[40] Albert M Sirunyan et al. Search for vector-like leptons in multilepton final states in proton-proton collisions at $\sqrt{s} = 13$ TeV. *Phys. Rev. D*, 100(5):052003, 2019.

[41] Stefan Bißmann, Gudrun Hiller, Clara Hormigos-Feliu, and Daniel F. Litim. Multi-lepton signatures of vector-like leptons with flavor. *Eur. Phys. J. C*, 81(2):101, 2021.

[42] Alexander Belyaev, Giacomo Cacciapaglia, Igor P. Ivanov, Felipe Rojas-Abatte, and Marc Thomas. Anatomy of the Inert Two Higgs Doublet Model in the light of the LHC and non-LHC Dark Matter Searches. *Phys. Rev. D*, 97(3):035011, 2018.

[43] Riccardo Barbieri, Lawrence J. Hall, and Vyacheslav S. Rychkov. Improved naturalness with a heavy Higgs: An Alternative road to LHC physics. *Phys. Rev. D*, 74:015007, 2006.

[44] D. S. Akerib et al. Projected sensitivities of the LUX-ZEPLIN experiment to new physics via low-energy electron recoils. *Phys. Rev. D*, 104(9):092009, 2021.

[45] LZ collaboration. First Dark Matter Search Results from the LUX-ZEPLIN (LZ) Experiment, 2022.